Shear Induced Tuning of Mechanical Properties and Ionic Conductivity of Composite Polymer Electrolytes

AN UNDERGRADUATE THESIS
submitted in partial fulfillment of the requirements
for the award of the degree of

Bachelor in Physics
DEPARTMENT OF PHYSICS
UNIVERSITY OF CRETE

by

Athanasios Machas
ph5408

Under the supervision of

George Petekidis
Professor

Emmanouil Glynos
Assistant Professor

July, 2023

This page was left intentionally blank

Figure 1: The Polymer and Colloid Group of IESL-FORTH (May 2023)

Acknowledgements

First of all, I would like to express my gratitude to my supervisors, Prof. George Petekidis and Prof. Manos Glynos for always being willing to help and to guide me, as well as for their patience with me when I messed up. Seeing polymer and colloid physics for the first time in my life through the minds of those two people, really sparked my curiosity and made me appreciate a branch of science that we physicists are notorious in looking down on: chemistry.

Secondly, I would like to thank the whole Polymer and Colloid group of IESL-FORTH (Figure 1), for being an amazing group of unique people who welcomed me, made me feel comfortable and made my stay pleasant. Special thanks to Vaso C. for bringing me here. Also many thanks to Georgia N. for answering my chemistry-related questions and for her guidance with most of the equipment I used, Katerina P. and Manos M. for their help on anything rheo-related and the technicians of the lab, Antje and Antonis. Finally, Lea F., Giannis S., Chrisostomos P. and Nikos B. for the great company.

A huge thanks should also be expressed to my friends Aias, Manos, Ioanna, Eleni, Apostolis and Spyros for supporting me and preferring to tell me of, rather than sugarcoating the pill. Sharing my undergraduate years with you was a pleasure.

Last but not least, thanks to my brother and my parents for their immense support throughout my studies, for hearing me for hours talking about my research without understanding a thing, yet still calling me the next day to check how my measurements went. Thanks for everything.

Abstract

The need for better and more sophisticated electrolytes for Li-ion batteries has been growing tremendously in the last two decades, due to the rapid developments in electric vehicles that require long lasting and safe batteries. Recent research examines whether polyelectrolytes from low molecular weight poly ethylene oxide (PEO) are a viable solution. PEO has inherently great ion conducting properties, yet its mechanical stability poses an issue. This problem can be addressed with the addition of nanoparticles that induce gelation. In this work, composite polyelectrolytes (CPEs) consisting of PEO with $M_w = 500$ gr/mol, hydrophobic fumed silica particles and Lithium bis(trifluoromethanesulfonyl)imide (LiTFSI) are studied, both on their rheological and electrochemical response. Also, preshear experiments are performed on the CPEs in order to further increase their mechanical stability and confirm that the shear tuning does not compromise the ionic conductivity.

Contents

List of Abbreviations

PEO	Poly Ethylene Oxide
CPE	Composite Polymer Electrolytes
LiTFSI	Lithium bis(trifluoromethanesulfonyl)imide
EIS	Electrochemical Impedance Spectroscopy
DSC	Differential Scanning Calorimetry
BM	Brownian Motion
FCC	Face Center Cubic
VdW	Van der Walls
SPE	Solid Polymer Electrolytes
DTS	Dynamic Time SWeep
DFS	Dynamic Frequency Sweep
DSS	Dynamic Strain Sweep
SAOS	Small Amplitude Oscillatory Shear
MAOS	Medium Amplitude Oscillatory Shear
LAOS	Large Amplitude Oscillatory Shear
LVE	Linear Viscoelastic
EV	Electric Vehicle

Chapter 1

Introduction

This section starts with explaining the need for solid electrolytes and a briefly presenting the current approaches on electrolyte design. Then, the materials used to compose electrolytes in this work are introduced and, after that, the experimental procedures used to assess the quality of our composites are described: Electrochemical Impedance Spectroscopy, Rheology and Differential Scanning Calorimetry.

1.1 Motivation: Solid Electrolytes

Since their invention, batteries have become an indispensable part of our everyday lives. All our portable devices (smartphones, laptops, headphones, wearables etc.) rely on compact, light weight, yet high performance batteries. The need for low size and high energy capacity energy storage devices, however, has grown significanly over the past decades, due to Electric Vehicles (EVs), whose main drawback, at the moment, is their insufficient mile range. The solution of this obstacle, requires designing batteries with higher gravimetric energy capacity, which means having higher energy storage capacity, per unit mass of the battery.

In figure 1.1, the fundamental components of a battery can be distinguished; the anode, the cathode (the two electrodes of the battery) and the electrolyte. The electrodes are where the redox reactions, necessary for creating charge carriers, occur. During discharge, ions flow from the anode to the cathode, whereas during charging, ions return to the anode and they are stored there. Hence, the capacity

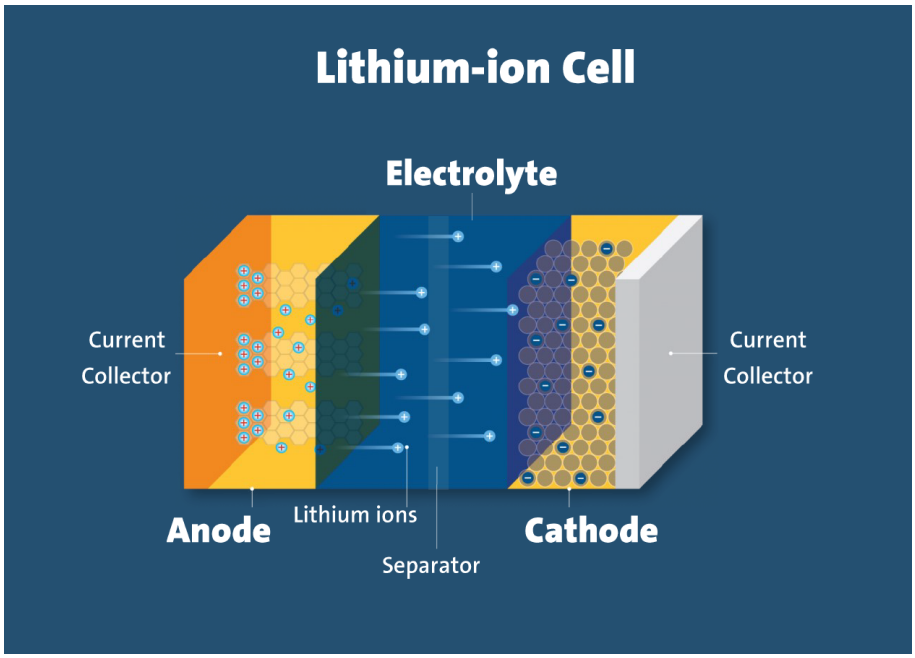

Figure 1.1: Schematic of a battery cell

of the battery is determined by the amount of ions the anode material can hold, so choosing appropriate ions and anode materials are of major significance.

The electrolyte is a substance or medium that facilitates the movement of ions between the battery's positive and negative electrodes (the cathode and the anode). It acts as a conductor for the flow of ions during the charging and discharging processes, while inhibiting the flow of electrons. Different battery technologies may employ different types of electrolytes, such as aqueous electrolytes (water-based), non-aqueous electrolytes (organic solvent-based), or solid electrolytes [1]. It plays a crucial role determining the overall performance of the battery including its capacity, energy density, power output, and overall stability.

Currently, lithium is the most promising element of the periodic table, in order to design high performance batteries. That is because Li has some unique advantages over the rest of the elements: first of all, its cation has one of the smallest ionic radii, which allows for fitting more of them in the same volume of anode material, compared to other elements. Additionally, it belongs to the first group of the periodic table (alkali metals), hence it is very electropositive and therefore, its corresponding salts will have a low dissociation energy. It is also the lightest of all alkali metals(the third lightest of all elements) and relatively abundant on earth's crust [2, 3]. Due to these innate characteristics of Li, lithium electrodes are capable of large charge

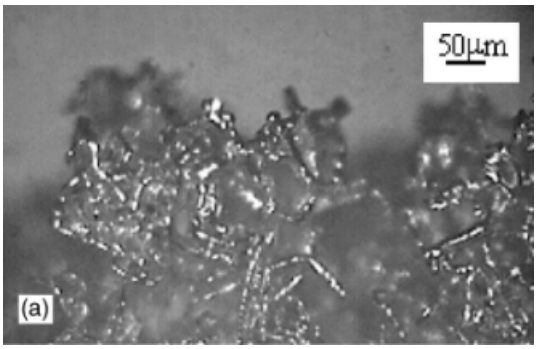

Figure 1.2: Lithium dendrites (image taken from [4])

capacity and high power density, rendering them ideal for energy storage solutions.

Having chosen lithium as the most promising ion for batteries, the question of what material to use for the anode arises, because that will ultimately be the deciding factor on the battery's capacity. The ideal choice would be crystalline lithium, because this structure is designed by nature to hold the maximum amount of lithium atoms in a given volume. Unfortunately, lithium electrodes have an major drawback: dendrites. Lithium dendrite formation (figure 1.2) is the most prominent mechanism that leads to the battery's degradation and malfunction. Dendrites are lithium crystalline structures forming on the electrolyte-electrode interface, that once nucleated, spread inside the electrolyte, reducing the number density of the lithium charge carriers and reducing the interface's contact surface, increasing cell's resistance. Dendrites can grow large enough, that the battery cell may eventually short circuit, leading to a large drop in resistance (lithium has an electron conductivity of $10^5 S/cm$, whereas the acceptable ionic conductivity for battery applications is $10^{-4} S/cm$), which finally results to huge currents running through the cell, posing fire hazards.

Since we want to design full lithium batteries, it is imperative we find a solution to dendrite formation. An efficient way to do so, is by mechanically suppressing them [4,5], i.e. using electrolytes with an elastic modulus of on the order of $\sim 1GPa$, comparable to that of crystalline lithium. Such moduli could be achieved by the crystallized polymer (under its melting temperature), but this significantly inhibits ion mobility in the electrolyte.

Solid Polymer Electrolytes (SPEs) are proposed as an elegant solution in order to combat lithium dendrite formation, while not substantially compromising ion

conduction. The recent approach is to compose inhomogeneous electrolytes from two distinct phases, one capable of high ion mobility and the other of great mechanical strength. Such composites could be made from block co-polymers (where one block offers high modulus and the other high mobility) [2, 6], or with the addition of inactive particles (like SiO_2, TiO_2 and clays) that form mechanically strong gels, swollen with a polyelectrolyte offering high ionic mobility.

The minimum requirements that need to be met for a solid-state electrolyte to be viable for Li-ion battery implementation are the following [4, 7, 8]:

1. **Ionic conductivity higher than 10^{-4} S/cm at 25^o C**: Essential in order to ensure reasonable charging and discharging power.

2. **Elastic Modulus around 1 GPa**: To provide structural stability but most importantly, to mechanically suppress the formation of lithium dendrites.

So, there are two main properties of the CPEs we would like to monitor and optimize: mechanical strength and conductivity. The former will be monitored experimentally with rheology, and the latter with Electrochemical Impedance Spectroscopy.

1.2 Matterials

The solid phase in the composites of this work will be formed by fumed silica particles. Fumed silica are SiO_2 particles are produced by flame hydrolysis of $SiCl_4$. The result is a light, fluffy powder (figure 1.3a)that consists of SiO_2 particles with diameter of 12 nm, that forms aggregates up to 200 nm in diameter (information from manufacturer). The aggregates are highly hydrophilic due to their coverage in SiO_2 so, in order to render them hydrophobic, some of the oxides are chemically replaced with non-polar molecules, rendering the aggregate non-polar, too. Fumed silica are widely used as a thickening agent. The fumed silica used here, the AEROSIL R202 (Evonic Industries) are coated with organosilane (figure 1.3b).

The liquid, amorphous phase will consist of PEO (figure 1.4) with a molecular weight of $M_r = 500$ gr/mol, that has both its ends capped with methyl groups (PEO-dm). This particular derivative of PEO was chosen, because both the low

(a) Fumed silica powder

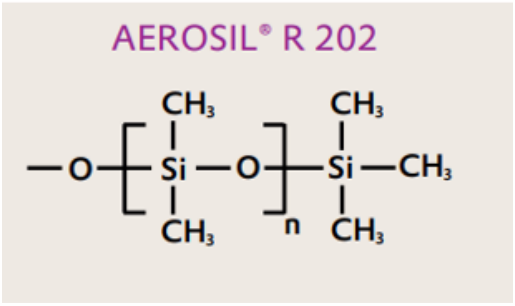

(b) The hydrophobic chain molecule attached at the surface of the hydrophobic fumed silica used in this work

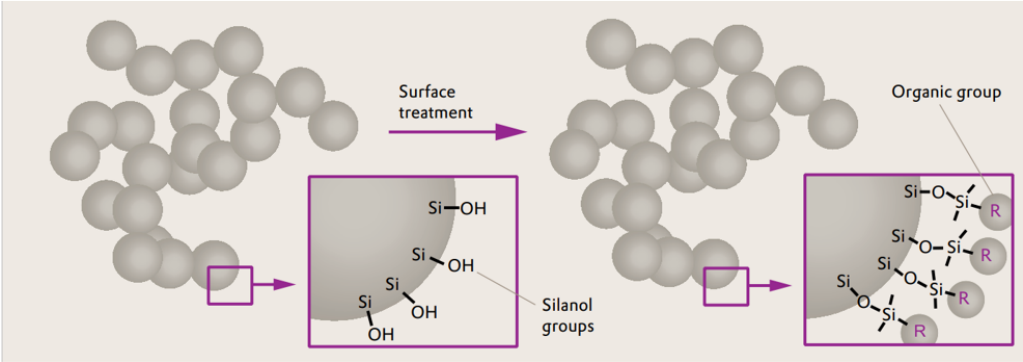

(c) Fumed silica aggregates

Figure 1.3: Images taken from Evonik Industries AG; AEROSIL Fumed Silica: Technical Overview

molecular weight and the methyl-capped ends increase the ionic conductivity [9], despite slightly lowering the elastic modulus [10], and it also enhances the interfacial properties with lithium elctrodes [11]. The weak mechanical properties of the low molecular weight of the PEO are of no concern, because the mechanical properties of the composites will be almost entirely determined by the solid phase, and so, we can choose the most conductive liquid phase we can. The lithium salt used here (LiTFSI), responsible for providing Li-ions in the electrolyte, was chosen due to its higher conductivity relative to the other lithium salt alternatives, because of its high degree of dissociation [12, 13].

1.3 Electrochemical Impedance Spectroscopy

In EIS, the sample to be measured is sandwiched between two electrodes and a low amplitude sinusoidal voltage is applied through them. Data is obtained for a wide range of frequencies (from 1 Hz to a couple of 1 MHz). By measuring the current that

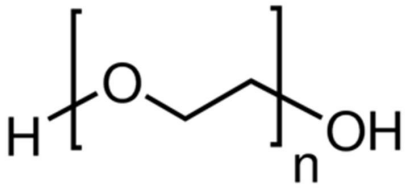

Figure 1.4: Poly Ethylene Oxide

is induced by the voltage, the complex impedance of the material can be calculated, by decomposing the current signal in a in-phase and an out-of-phase component. The in-phase impedance corresponds to bulk resistances in the material, whereas out-of-phase components are created from (but not limited to) the capacitance of the electrodes, the sample-electrode interface and capacitance that rises from the different orientations of the crystalline regions in the sample. In very high frequency regime, inductance phenomena can also appear [14].

The results are often presented in a Nyquist plot (figure 1.5)(a graph with the x axis corresponding to the real part of the impedance Z' and the y axis corresponding to the imaginary part Z''). Usually, the y axis is inverted so the capacitance effects would be more prominent on the first quadrant. In the scope of this work, the most important data obtained from the EIS is the bulk resistance, which is the value of Z' when Z" is zero. When the real and imaginary parts of the complex impedance function are plotted against frequency, the value of the DC bulk resistance R_b is the value of the real part of Z in the frequency independent region 1.6. The importance of R_b is due to the fact that the polyelectrolytes studied here are designed for DC batteries.

1.4 Rheology

Rheology is a scientific discipline that investigates how materials deform when stresses and forces are applied to them. There are various types of rheological experiments, such as shear, extensional and compression experiments, depending on the way the stresses are applied to the material. The ones relevant to this work

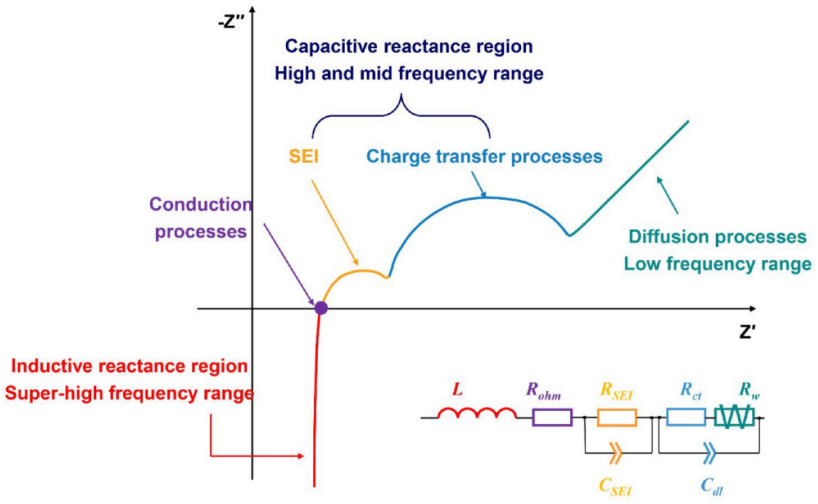

Figure 1.5: Example of the Nyquist plot produced from a polymer electrolyte and its equivalent circuit, designed using resistors and capacitors

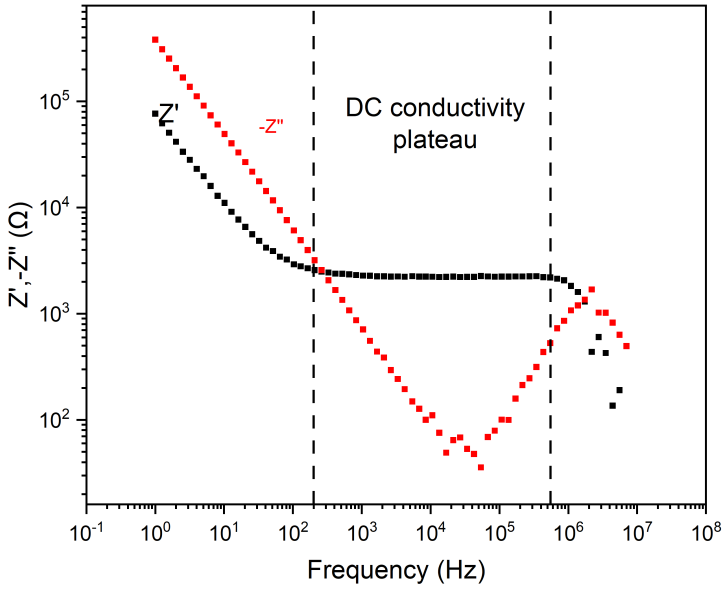

Figure 1.6: Impedance spectrum of the 2% w/w R202-PEO composite with r=0.055 LiTFSI

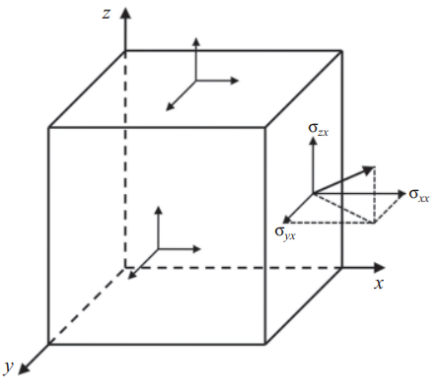

(a) A visualization of the 3D stress tensor. The shear stresses are σ_{ij} where $i \neq j$

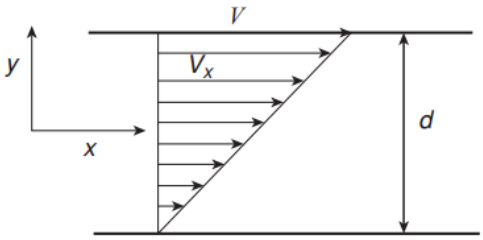

(b) A typical flow profile in a shear experiment; the material flows in the x direction, yet the velocity has a gradient in the y direction

Figure 1.7: Schematics from [15]

is the shear rheological experiments, which are the only ones discussed thoroughly in this section. Rheological measurements provide valuable insights into the internal microstructure, viscoelastic properties, and flow characteristics of materials like liquids, polymer solutions, melts, colloidal suspensions, glasses and gels.

1.4.1 Shear rheology

The two most fundamental concepts of shear rheological experiments are shear strain γ and shear stress σ. In simple terms, γ is defined as the ratio of the displacement of the top plate in Figure 1.7b, over the thickness d of the sample $\gamma = \Delta x/d$, and shear stress is a mechanical force F that acts perpendicular to the surface of an object or material with area A, $\sigma = F/A$. Both definitions consider that the material consists of adjacent layers that slide or move relative to each other in response to an applied force.

Rheological experiments are conducted in devices called rheometers, and in order to perform shear rheological experiments, rotational rheometers are used. Strain-controlled rheometers consist of two plates: one that is able to rotate about a horizontal axis using a motor and is the one that applies the shear strain or stress, and an immobile plate that is connected to a transducer, a device capable of measuring the torque exerted on the plate. The sample under measurement stands in between these plates. Hence, the motor applies a shear strain to the material which results

to a stress that the transducer records, so we can relate strains or strain rates with stresses. On the contrary, in stress-controlled rheometers, the sample rests on a plate and the same tool is able to move and measure the exerted torque. These rheometers, when in strain-control mode, manage to apply specific strains through a feedback loop.

1.4.2 Strain-Stress relations from classical theories

The relationship of the shear stress versus shear strain of an ideal solid is modeled by Hooke's Law (1.1). The proportionality constant G is called the elastic modulus.

$$\sigma = G\gamma \tag{1.1}$$

In contrast, in an ideal fluid the stress is proportional not to the strain, but to the rate of strain, according to Newton's Law (1.2). The proportionality constant η, is now the viscosity of the material.

$$\sigma = \eta\dot{\gamma} \tag{1.2}$$

1.4.3 Steady shear experiments

In steady shear experiments, the rheometer applies a constant rate of deformation $\dot{\gamma}$, also called "rate" for short, and measures the stresses created. A common experiment is to perform a rate sweep test, i.e. recover the steady state value of the stress for different rates. Results of such tests are presented in Figure 1.8. The Herschel-Bulkley model [16](1.3) describes the behaviour of a generalised non-Newtonian fluid and encapsulates phenomena such as thickening, thinning and yield stresses.

$$\sigma = \sigma_y + \eta_{pl}\dot{\gamma}^n \tag{1.3}$$

The most common steady shear experiments are:

1. **Steady Rate Sweep**: subjecting the sample in various different shear rate deformations and measure the shear stress response of the material, while also calculating its viscosity

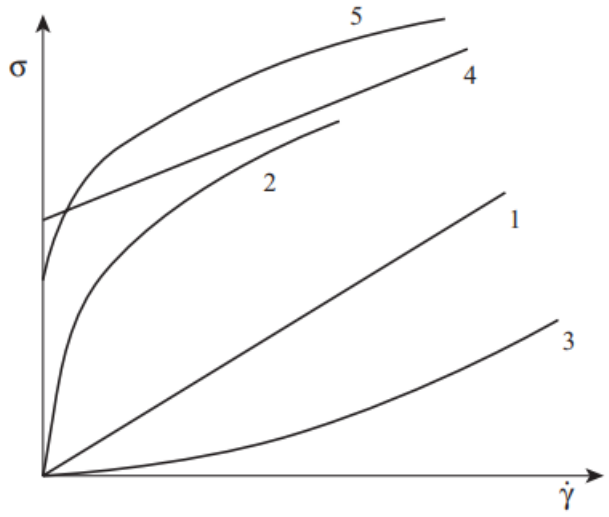

Figure 1.8: Shear stress versus shear rate for: (1)Newtonian fluid, (2) Shear Thinning fluid, (3) Shear Thickening fluid, (4),(5) Materials with yield stress

2. **Step Rate**: while the sample is at rest, instantly apply a constant shear rate on it and observe how stress evolves over time

1.4.4 Oscillatory shear experiments

In oscillatory measurements, the rheometer exerts a sinusoidal strain on the material like in 1.4.

$$\gamma = \gamma_0 sin(\omega t) \tag{1.4}$$

Therefore, if the material is purely elastic, Hooke's Law (1.1) dictates that the stress will also be sinusoidal and in phase with the strain (1.5)

$$\sigma = G\gamma_0 sin(\omega t) \tag{1.5}$$

If however the material is purely viscous, by Newton's Law (1.2), the stress will be ninety degrees ahead of the strain (1.6)

$$\sigma = \eta\omega\gamma_0 cos(\omega t) = \eta\omega\gamma_0 sin(\omega t + 90^o) \tag{1.6}$$

For a material that has both elastic and viscous properties (i.e. viscoelastic), at low strains, the stress will obey equation 1.7

$$\sigma = \sigma_o sin(\omega t + \delta) \tag{1.7}$$

So, by decomposing the stress in an in-phase and an out-of-phase component, by substituting $G' = G$ and $G'' = \eta\omega$ on 1.5 and 1.6 and using complex numbers, we can define the complex modulus

$$\sigma = G^* \gamma_0 sin(\omega t) = G^* \gamma \tag{1.8}$$

$$G^* = G' + iG'' \tag{1.9}$$

G' is called the storage modulus and G" is called the loss modulus. Their unit of measurement is the Pascal.

The most common oscillatory shear experiments are:

1. **Dynamic Time Sweep**: apply a constant strain amplitude and a constant frequency on the sample and observe the growth of the storage and loss moduli over time

2. **Dynamic Frequency Sweep**: perform measurements of the storage and loss moduli at various frequencies while keeping the strain amplitude constant

3. **Dynamic Strain Sweep**: measure both moduli at a constant frequency for various strain amplitudes

1.5 Differential Scanning Calorimetry

DSC is an extremely useful technique in order to study the thermodynamic properties of a material. Its fundamental principle is quite simple: observing the heat flow of the material while changing its temperature. If, for example, the melting temperature of the material is reached, heat flow will spike, as melting is a highly endothermic procedure. Therefore, using DSC, quantities like glass transition temperatures, melting and crystallization temperatures and the degree of crystallinity can be experimentally found.

When discussing the impedance or the bulk conductivity of a material, it is vital to also know its thermodynamic behaviour, especially when it comes to a

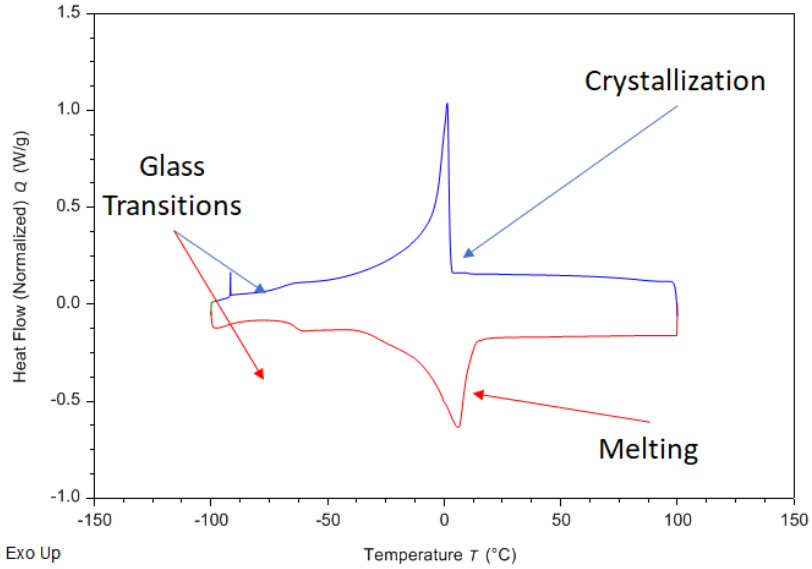

Figure 1.9: Example of a DSC cycle. In this case positive heat flow corresponds to an exothermic reaction. While cooling, a crystallization peak is observed and while heating a melting peak appears. Heat flow remains mostly constant throughout the whole cycle (and so does the C_p). The sudden change in the level of the heat flow indicates a glass transition

polymer. This is because glass transitions and crystallization affect the microscopical arrangement of the polymer chains tremendously. For example, crystallinity needs to be avoided, as ion conduction takes place primarily in the amorphous phase [17, 18]. Crystallization of the PEO is the main property of our composites that we want to monitor and prevent.

1.6 Colloidal Systems

1.6.1 Definition

A colloidal system is defined as a mixture of two insoluble substances. We can distinguish the continuous phase, the matrix in which the colloidal particles are suspended into, which are also called the dispersed phase. There are many classifications for colloidal dispersions, such as sols (a solid phase dispersed in a liquid phase), gels (a liquid phase dispersed in a solid phase), liquid aerosols (a liquid phase dispersed in a gas) and more. Colloids have a wide variety of uses both in everyday products and for industrial materials.

It is highly important for a colloidal dispersion that the suspended particles have a size ranging from a few nanometers to a few micrometers. This parameter is quite crucial, because it dictates the governing force in the system: Brownian motion. Brownian motion (BM) is the random walk movement of the suspended particles, caused by the multiple thermal collisions occurring between these particles and the smaller particles of the solvent. In such systems, we refer to the diffusion of the particles, which correlates the mean square displacement of the particles with time, and in three dimensions is expressed using 1.10.

$$\langle \Delta r^2 \rangle = 6 D_0 t \tag{1.10}$$

For a colloidal system where the viscosity of the medium is η_m and the particle radius is R, the diffusion coefficient D_0 is calculated using the Stokes-Einstein relation (1.11).

$$D_0 = \frac{k_B T}{6\pi\eta_m R} \tag{1.11}$$

where k_B is the Boltzmann constant and T is the absolute temperature.

1.6.2 Hard Sphere Colloids

The most simple colloidal system we can study is that of hard spheres. Here, the suspended particles have a radius of R and do not interact with each other, yet they occupy space, hence they cannot overlap (this kind of interaction is known as excluded volume interaction). The interparticle potential can be expressed as

$$V_{int}(r) = \begin{cases} 0 & r > R \\ \infty & r \leq R \end{cases} \tag{1.12}$$

In such a potential, temperature has no effect in the phase state of the system and the only parameter that should be considered is the volume fraction ϕ. The volume fraction is defined as the ratio of the volume of the suspended particles, over the total volume of the system (1.13)

$$\phi = \frac{V_c}{V} = \frac{V_c}{V_c + V_m} = \frac{4}{3}\pi R^3 \frac{N}{V} \tag{1.13}$$

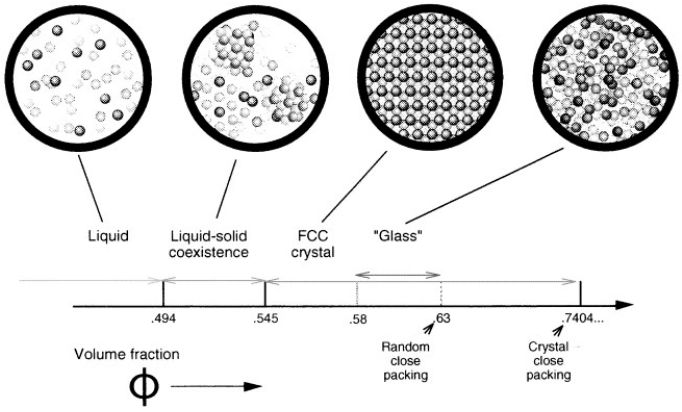

Figure 1.10: **Phase Diagram of Hard Sphere Colloids.** At sufficiently low volume fraction ($\phi < 0.494$), BM drives the system to equilibrium by achieving a uniform density, resulting in a liquid system. Above $\phi = 0.545$, entropy drives the system to a face center cubic (FCC) crystal. In between there coexists both a liquid and a crystalline phase. Between $0.58 < \phi < 0.638$ the system is in a glass state and at $\phi = 0.638$ it reaches the random close packing volume. Maximum packing is achieved at $\phi = 0.74$ with a FCC arrangement. [15]

where V is the total volume of the system, V_s is the volume of the solvent and N is the number of the suspended particles. Using ϕ as a parameter we can construct the phase diagram of a hard sphere colloid system (Fig 1.10)

1.6.3 Interactions

There are many interactions that can influence the phase behaviour of a colloidal system, such as electrostatic interactions, Van der Walls (VdW) interactions or steric effects. The two former ones in an aqueous solution in the presence of ions have been described by the Derjaguin-Landau-Verway-Overbeek potential (DLVO for short). This model incorporates the induced VdW interactions and the shielded by the ions electrostatic potential between the charged particles. Particle interactions, though, are the reason why the phase diagrams of real systems are not as simple as 1.10, and dependent on temperature, pH or the presence of ions. The interactions of the dispersed particles with the particles of the medium and the interparticle interactions are the determining factors on whether the system will end up as a suspension, or it will percolate and form structures. Since the scope of this work is for the solid phase to achieve high elastic moduli, we seek for the dispersed particles to percolate.

The dominant forces in the systems studied in this work are hydrophobic interactions [10], which are essentially VdW forces. These kind of interactions occur

when non-polar (hydrophobic) particles are dispersed in a polar (hydrophilic) continuous phase. In such systems ,the hydrophobic particles attract to each other and form aggregates because in that way, they reduce their contact surface with the hydrophilic phase, which is unfavorable from the entropic side, but favorable from the enthalpic side. So, due to the fumed silica particles being suspended in a bad solvent, percolation of the system is achieved.

Chapter 2

Experimental

2.1 Goals

The first goal of this work is to study the materials consisting of PEO and fumed silica, uncover their interactions and examine the effect of the silica volume fraction on the mechanical stability of the material. The next stepping stone is to examine the same properties on the PEO-silica plus LiTFSI blends, while also measuring their conductivity at rest.

The final and main objective is to attempt to tune the mechanical and electrochemical properties of the CPEs using shear. More specifically, it is known from previous works [19, 20] and figure 2.1 that similar systems can have their mechanical properties vary, by applying various shear deformations on them. This happens due to the fact that different non-linear deformations cause different structural rearrangements and bond breaking in the sample, and therefore, result in higher or lower elastic moduli. That dependence on various shear deformations is examined in parallel with the conductivity of the sample and it is of major concern whether the conductivity is compromised, while the mechanical stability is increased by shear induced tuning.

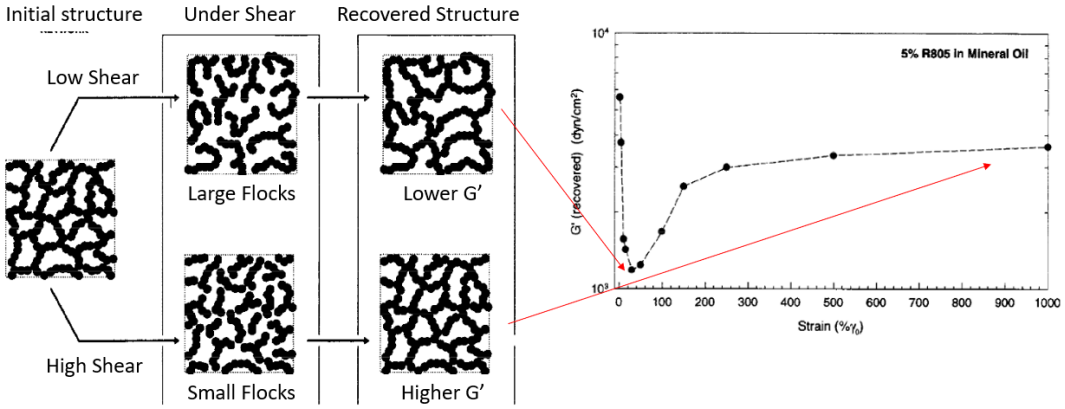

Figure 2.1: Tuning Schematic, taken from [19]

2.2 Synthesis of CPEs

PEO was mixed with the fumed silica in various weight fractions (ranging from 2% to 10%) resulting in volume fractions from around 1% to 5%. All samples where mixed overnight using a magnetic stirrer until homogeneity was reached. For weight fractions above 5% where the samples were too viscous to stir, a co-solvent (acetonitrile) was used in order to ensure mixing was effective. The co-solvent was dried in vacuum oven at an elevated temperature above acetonitrile's boiling point (80^o C) and its evaporation was checked by weighing the sample, before and after the drying in the oven. Furthermore, all samples were left overnight in vacuum before any rheological measurements, in order to remove any air bubbles in the mixture.

The addition of the lithium salt and the storage of the resulting blends was done in an argon-filled glove box, due to the salt's volatility in humidity. The appropriate amount of LiTFSI was added to the PEO-silica mixtures in order to achieve a molar ratio of 0.055 between the Li and the O molecules of the PEO. This ratio achieves the maximum conductivity in oligomeric PEO [21]. The blends were left one day in vacuum, and another day in vacuum with elevated temperature in order to ensure the evaporation of the co-solvent.

2.3 Experimental Procedure

The first series of experiments that were performed was the characterization of the PEO-silica mixtures without the lithium salt. This was done in order to uncover the

interactions between the PEO chains and the silica particles, but most importantly to study the effect that the lithium salt has on these interactions.

The interactions and the microstructure of these systems where studied using rheology. The experiments were done in a stress-controlled Anton Paar Physica MCR 501 Rheometer, using a cone-plate geometry with a diameter of 50 mm, and a diameter of 25 mm for weight fractions above 7%. First, a Steady Rate Sweep test and a DSS test were performed, the former to find the rate at which the sample exhibits the lowest viscosity, and the later to discover at which strain amplitudes the response of the sample is linear. Both of these findings were used to construct a rejuvenation protocol, that will later be used to erase shear history between measurements and ensure reproducible results. The rejuvenation consists of applying a steady rate (that of the minimum viscosity) for 100s, followed by a DTS test, applying an angular frequency of 1 rad/s and a strain amplitude in the linear range, for as long as required to achieve steady state (the G' and G" no longer evolve over time). Then, a DFS test was performed in order to probe its viscoelastic response, again with a strain amplitude in the linear regime. A linear strain is mandatory, so as not to disrupt the structure that has been created, but rather, examine it at rest.

DSC measurements were taken using a DSC-25 (TA Instruments) in an aluminum pan. The temperature range varied from -100^{o}C to 100^{o}C at a rate of 10^{o}C/min. Two cycles from 100^{o}C to -100^{o}C and then to 100^{o}C where executed. Whenever the sample crystallized during the cooling step, in the cooling step of the next cycle a 30^{o}C/min rate was applied until the crystallization onset, from there the rate was set to 60^{o}C/min until the end of crystallization and lastly, -100^{o}C were reached with 30^{o}C/min. This procedure (hereby called quenching), is an effort to inhibit crystallization. If quenching did not work, the glass transition temperature T_g was not considered accurate, since the sample is semi-crystalline and only the amorphous phase exhibits a glass transition. Instead, the crystallinity index can be calculated, which is defined as the percent weight of the PEO that is crystallized. To calculate the crystallinity index we take advantage of the melting of the crystalline phase during the heating step. By integration of the heat flow when this melting occurs, we can extract the enthalpy of melting, normalize it with the weight percent of the PEO in the sample and compare it with the enthalpy of melting of the fully

crystallized PEO.

Then, the rheology of the PEO-silica-LiTFSI blends was done using a strain-controlled ARES melt rheometer, using a plate-plate geometry with a diameter of 8 mm. A Rheo-EIS setup was used in order to correlate the rheological properties with the conductivity of the CPE. Straight after loading, a DSS test was conducted to pinpoint the linear regime of each sample and then a DFS test was executed to probe its structure, followed immediately by an impedance measurement. Steady shear experiments were difficult in this setup due to the fracture of the material, causing it to get ejected out of the plate-plate geometry.

Tuning by shear was attempted, first on the PEO-silica samples and then on the PEO-silica-LiTFSI blends. Both oscillatory and steady preshear protocols were studied. In both cases, a rejuvenation protocol was devised, then a steady or oscillatory preshear was applied and finally, a linear DTS was performed in order to observe the storage modulus obtained after the preshear. Right at the end of the DTS, an impedance measurement was taken and then the rejuvenation would start again, to prepare the sample for the next preshear.

Figure 2.2: The Rheo-EIS setup

Chapter 3

Results

3.1 PEO-Fumed Silica Composites

In this section the rheological properties of the composites containing the PEO and the hydrophobic fumed silica are discussed. The frequency sweeps for the composites in various weight fractions are presented in Figure 3.1. It is apparent that for all weight fractions, the storage modulus is frequency independent for a wide frequency window. This rubbery plateau is indicative that a three dimensional network has formed in the material by the silica particles. For the sample containing 2% silica, we observe a crossover of G' and G" in the high frequency regime, after which the material becomes liquid-like. This is a sign of the material having glassy properties. For higher weight fractions, G" flattens out and becomes frequency independent, too, but nonetheless remains at least one order of magnitude lower than G'. This solid-like behaviour of these samples can also be visually validated. For weight fractions above 5%, samples appear to be transparent gels, whereas for samples below 5%, they flow under rotation of their container.

Next, the non-linear behaviour of the composites are explored, by performing Dynamic Strain Sweeps (Figure 3.2). The first thing we observe in all samples is the existence of a linear plateau in the Small Amplitude Oscillatory Shear regime (SAOS regime). This is where the material exhibits a classical, Hooke-like behaviour (1.1), where the storage modulus is independent of the applied strain, and it defines

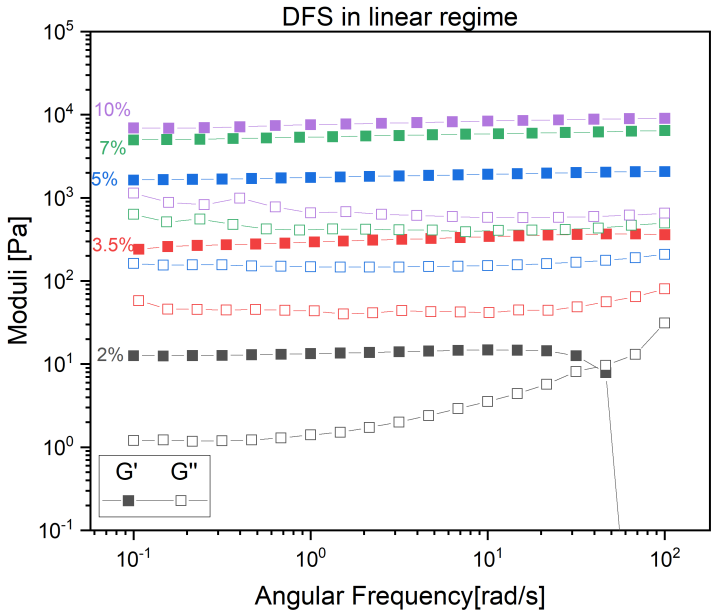

Figure 3.1: Dynamic Frequency Sweeps in linear regime for 1%, 3.5%, 5%, 7% and 10% weight fraction of AEROSIL R202 in PEO-dme 0.5k

Weight Fraction	$\gamma_{co}(\%)$
2%	6.81
3.5%	0.86
5%	2.15
7%	1.58
10%	0.89

Table 3.1: Crossover strain at 1rad/s

the Linear Viscoelastic (LVE) regime.

The end of the plateau marks the start of the Medium Amplitude Oscillatory Shear (MAOS) region, where the material starts to yield. The start of the MAOS regime seems to progressively shift towards lower amplitudes, as the weight fraction of the silica particles increases. The same holds true for the crossover point of G' and G" in the strain sweep (γ_{co}) (With the exception of the 3.5% sample). The values of the crossover strains are presented in Table 3.1. We can also observe a peak at G" near the crossover point. This is indicative of high structure decomposition and bond breaking.

Also, in order to properly examine the particle interactions that lead to gelation of these systems, the storage modulus of each sample at a given frequency (1 rad/s), was taken from the linear DFSs and plotted against the volume fraction. Theoretical

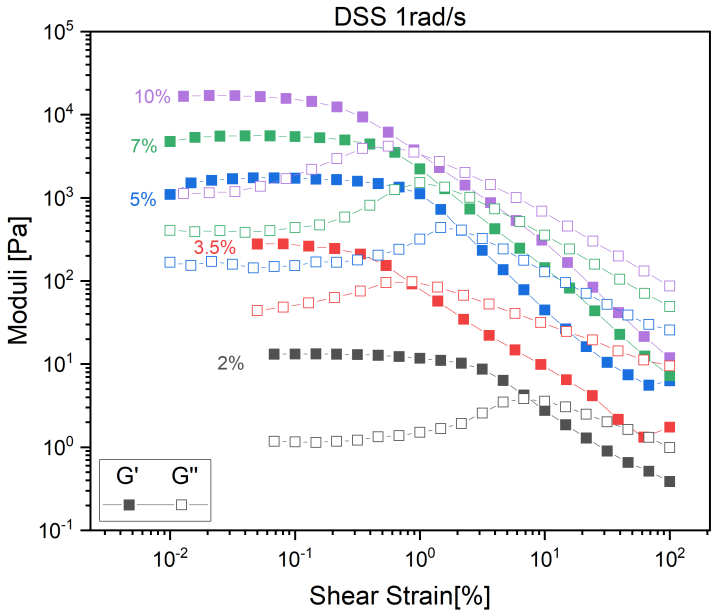

Figure 3.2: Dynamic Strain Sweeps at 1 rad/s for 1%, 3.5%, 5%, 7% and 10% weight fraction of AEROSIL R202 in PEO-dme 0.5k (measurements at values lower than 0.1% strain amplitude for the 2% and 3.5% samples have not been taken due to torque limitations)

analysis and experiments on fractal gels, such as the ones studies here, are reported to show a power law dependence of the volume fraction on the G' [22–24]. So, in a log-log graph (Figure 3.3), the fitted slope has a value of 4.3 ± 0.3, and therefore the storage modulus scales as

$$G' \sim \phi^{4.3\pm0.3} \tag{3.1}$$

In similar systems, the exponent takes values of 4.0 ± 0.5 [24] and 4.4 ± 0.2 [22].

3.2 Addition of LiTFSI

The next step is to examine the effect of the LiTFSI addition on the rheology of the samples. We take as an example the composites containing 10% fumed silica. First we compare the Dynamic Frequency sweeps with and without LiTFSI (Figure 3.4). Both samples exhibit a frequency independent G' plateau, yet it is apparent that the addition of salt, increases the G' by a factor of ten (consistent with [9, 25]. This increase can be explained if we consider the hydrophobic interactions between the fumed silica particles: the dissociation of salt ions renders the polymer matrix more

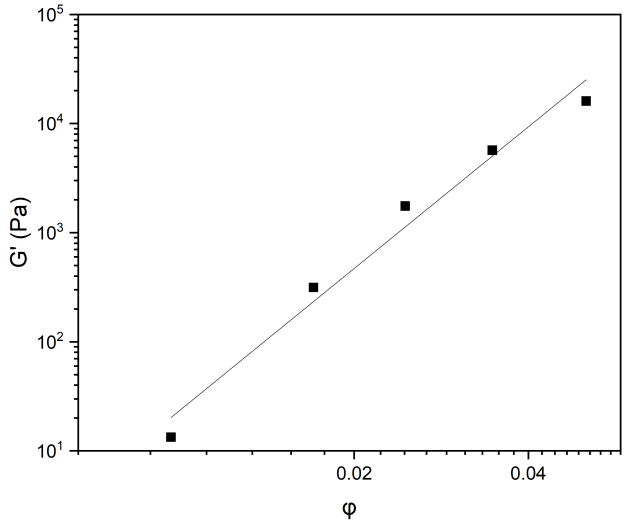

Figure 3.3: Scaling of storage modulus with volume fraction in the PEO-Silica composites, with no Li salt

hydrophilic, because its polarity increases, and therefore the hydrophobic attractions become more significant.

The effect of the salt addition, though, does not remain that significant, as the weight fraction of the silica decreases. As observed in Figure 3.5a, at the highest volume fraction the sample with Li salt has a greater value of G', yet at the intermediate value of ϕ, the salt addition barely changes G'. At even lower values of ϕ, G' decreases with addition of salt. A possible explanation can be formulated if we consider that the microstructure is formed by silica aggregates. While adding salt in low volume fractions, particles aggregate due to their fractal nature, they overlap and their effective volume decreases. After a certain concentration, however, the aggregates are dense enough in the medium that they can start forming bonds with each other, thus increasing G' at higher volume fractions. Nevertheless, the power law dependence of ϕ on G' seems to shift from $G' \sim \phi^{4.3\pm0.3}$ for the no-salt case, to a $G' \sim \phi^{6.5\pm0.4}$ for the samples containing Li salt, which agrees with the observation that the ions do indeed increase the hydrophobic interactions (Figure 3.5a).

Another interesting result can be drawn by inspecting Figure 3.5b, which shows how both the storage modulus of the frequency independent plateau and the at-rest conductivity of the PEO-silica-LiTFSI composites, vary while increasing the silica weight fraction. By increasing the weight fraction from 3.5% to 10%, we can enhance

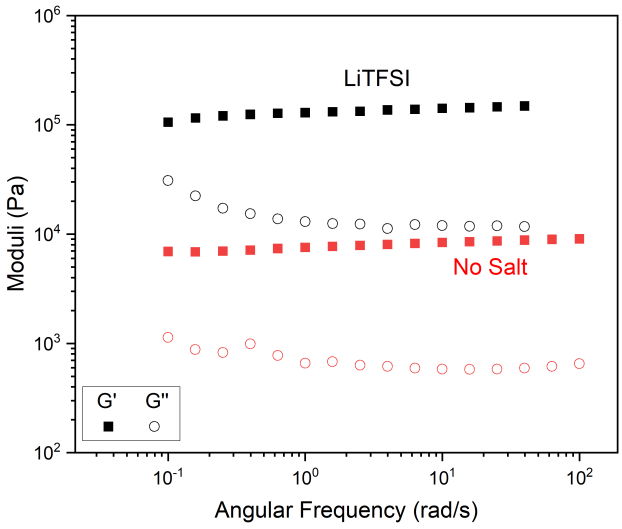

Figure 3.4: Comparison of the frequency sweeps of 10% R202 in PEO 0.5k dme, with and without LiTFSI

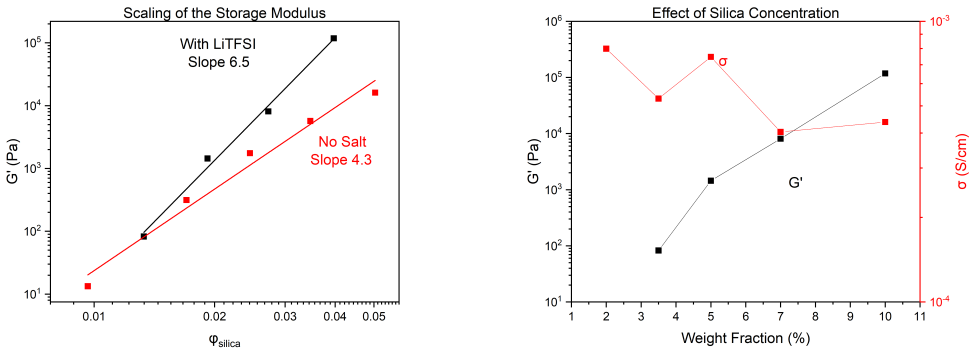

(a) Storage moduli taken from the DFSs at 1 rad/s for every volume fraction, with and without LiTFSI

(b) Storage moduli and conductivity values for various volume fractions for the PEO-silica-LiTFSI composites

Figure 3.5: Effect of Salt addition

the mechanical strength by three orders of magnitude, while the conductivity drop is negligible (0.5 fold). This implies that the mechanical and the electrochemical properties of the composite polyelectrolytes are effectively decoupled. This can be attributed to the open structure formed by the fumed silica that does not impede ion diffusion [25]. Hence, we shall be able to enhance the mechanical properties by adding more silica particles or by tuning, while not risking the conductivity dropping dramatically, thus making the electrolyte not suitable for EV applications.

3.3 DSC tests

Both cooling and heating steps for various silica contents of the silica-PEO composites, with and without salt are presented in Figures 3.6 and 3.7. From the cooling steps, we can confirm that every sample with no salt except the 10% and every one with LiTFSI except the 10% and the 7%, crystallized. Quenching was attempted but crystallization was not prevented. Therefore, the only glass transition temperatures we are confident about, are the following: -69.85^{o}C for the 10% with no salt, -58.29^{o}C for 10% with LiTFSI and -76.93^{o}C for the 7% with LiTFSI. However, we can plot the degree of crystallinity as a function of the silica weight fraction (Figure 3.8). As expected from similar works, crystallinity is reduced with the addition filler particles [26, 27], which in this case refer both to the fumed silica and the lithium salt. We can also observe that the crystallinity index of the samples is for the most part constant for weight fractions before 5% and then, it drops abruptly. This can be explained considering the mechanism that prevents crystallization of the PEO: confinement. At low weight fractions, crystallization is hindered because impurities in the PEO crystalline phase are introduced to the existence of non-PEO particles, which increase the energy of the crystal. However, after sufficient silica concentration, crystallization is inhibited because the polymer is forced to crystallize in a narrow, confined space, inside the fractal gel structure formed by the fumed silica. Another, maybe more naive approach, would be to observe that if the crystallinity data for the 5% samples, crystallinity would drop monotonically. So, a mistake during the experiment could be a possibility, too. In order for the crystallinity index to be higher than expected, fewer filler particles should have been added. However,

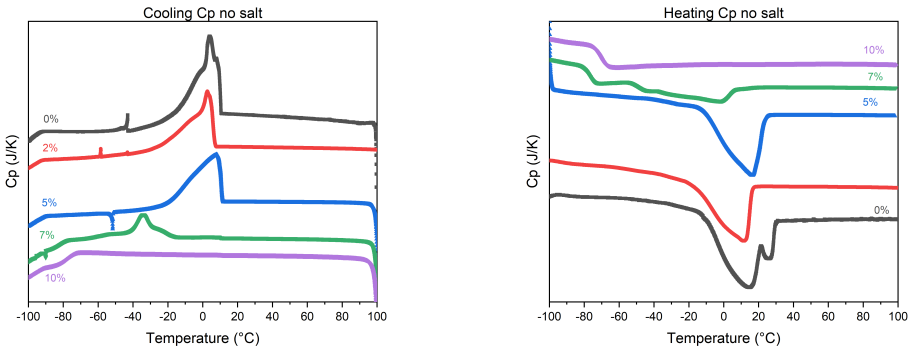

Figure 3.6: DSC for the composites without salt

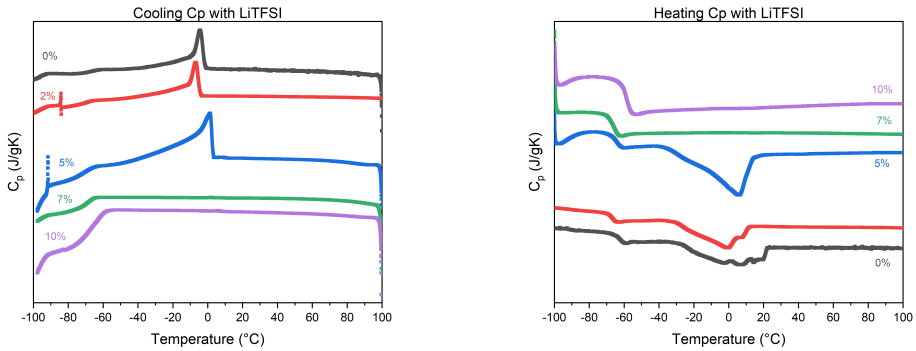

Figure 3.7: DSC for the composited with r=0.055 LiTFSI

we can confirm from figure 3.5b that the proper amount of silica particles should have been added (because the G' of the 5% composite falls in place) and the proper amount of LiTFSI has been added (maybe even more), since the conductivity for that sample also fits with the rest of the data. In any case, this behaviour should be extensively studied again, in order to figure out whether the 5% samples were properly measured and no mistake has been made. Nevertheless, since the only samples with salt that are not prone to crystallization are the ones containing 10% and 7% fumed silica, these should be the most suitable for electrolyte applications.

3.4 Tuning by shear

Since we established that the electrochemical and the mechanical properties of the composite polyelectrolytes are, for the most part, independent, the next step would be to attempt to tune the mechanical properties of the composites by shear, yet always making sure we do not sacrifice on conductivity. In order to examine the

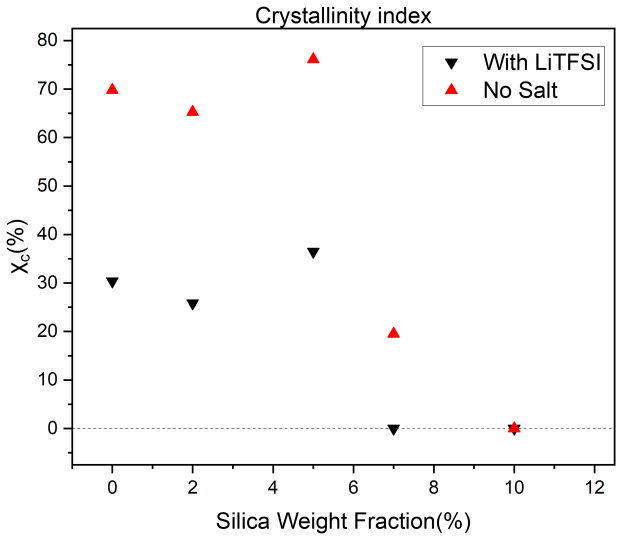

Figure 3.8: Degree pf Crystallinity

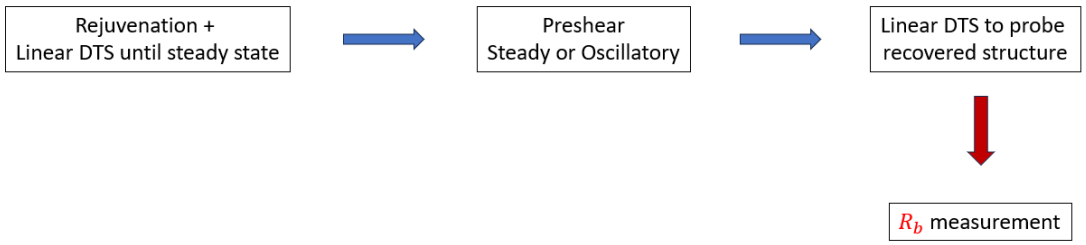

Figure 3.9: The Tuning Protocol

tunabiliy of the samples, a tuning protocol is devised: a rejuvenation is necessary to ensure reproducible results (either at a high steady rate or a large amplitude oscillatory shear for a given time, and then a linear DTS), followed by the preshear (again, either steady or oscillatory) and at last a final linear DTS in order to probe the microstructure. Right at the end of the DTS, an impedance spectrum is captured, so as to correlate the mechanical and the electrical properties of the material (Figure 3.9).

At first, the tunability of the 10% silica-PEO composite with no salt is tested. First with a 1h long oscillatory preshear (Figure 3.10a), and then with a 5 min steady preshear (Figure 3.10b).

Shear induced tunability of colloidal gels has been demonstrated in previous studies [19,20,28,29]. As seen in figures 3.10a and 3.10b, tuning by shear is effective

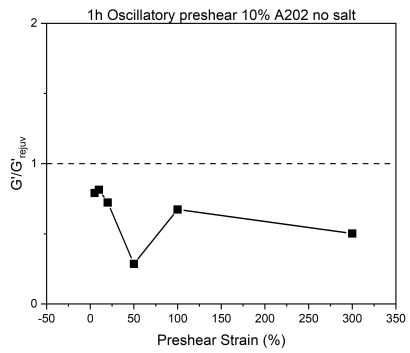

(a) 1h of oscillatory preshear. The rejuvenation was 1 minute of steady shear at 200 s^{-1}, the DTSs were at 1rad/s and 0.05 strain amplitude, both for 1h and the preshear was applied at a frequency of 1 rad/s

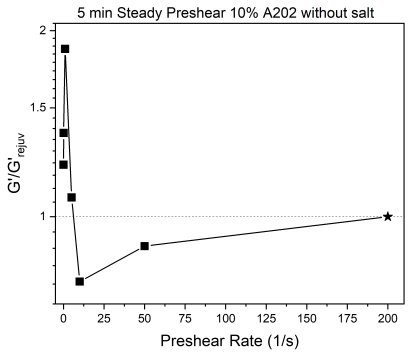

(b) 5 min of steady preshear. The rejuvenation was 1 minute of steady shear at 200 s^{-1}, and the DTSs were at 1rad/s and 0.05 strain amplitude for 15 minutes

Figure 3.10: Tuning (steady and oscillatory) of 10% R202 in PEO-dme 0.5k

on the 10% composite, especially the steady preshear. At low preshear rates, the recovered G' increases dramatically, almost by a factor of 2. This is can be explained by considering that low preshear rates do not cause significant structure breakdown, but, instead, allow the sample to "explore" its possible structural configurations, ultimately finding the one with the lowest energy. The lowest energy configuration is the one where the aggregates are surrounded by the maximum number of neighbouring aggregates, feeling maximum attraction and, consequently, resulting in the strongest gel. Then, as preshear rate is increased, structure breakdown starts to occur, hence the drop on the recovered modulus. Lastly, at high enough preshear rates, the aggregates start to get broken down too, which means that, after cessation of the preshear, the recovered structure will be comprised of smaller aggregates, resulting in a denser and stronger network. Oscillatory shear does also have an effect, but it is less prominent and the ratio of G' after preshear over G' after rejuvenation stays below one. The reason behind this behaviour is that oscillatory shear is not as effective as steady shear, when it comes to breakdown of the aggregates. So, after the initial high shear, the rejuvenated structure as strong as it possible. At high enough strain amplitudes (maybe in the order of 10^3% or even 10^4%), oscillatory shear would achieve higher aggregate breakdown than the $200s^{-1}$ rejuvenation, and therefore, result in recovered moduli above 1. This system could be examined in

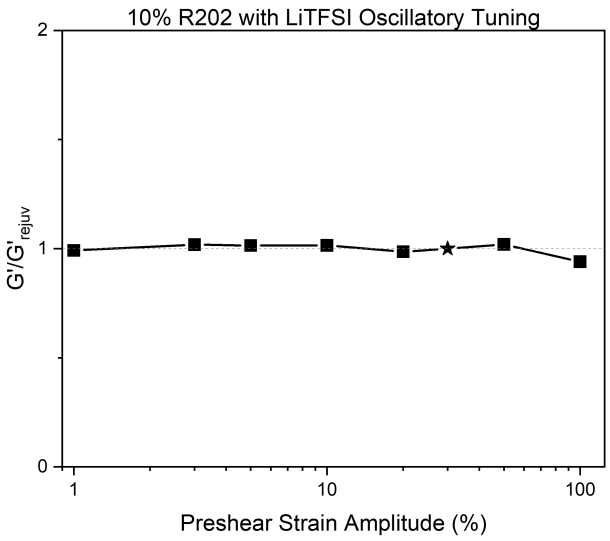

Figure 3.11: Oscillatory tuning of 10% silica-PEO-LiTFSI. The rejuvenation was done by applying a 30% strain for 2 minutes, and then a DTS at 0.2% strain after the rejuvenation and preshear. The frequency was always 1 rad/s

more detail, yet here the objective involves tuning of the composites with salt, in order to account for the conductivity, too.

At first, the tunability of the 10% R202 in PEO with LiTFSI was studied. Steady shear experiments were not conducted, due to shear fracture, so only oscillatory preshear was tested (Figure 3.11). Again, due to fracture limitations, the maximum shear amplitude used was 100%. It is evident that this particular sample is insensitive to tuning (the largest deviation from G'_{rejuv} is 6% at 100% strain). This might have been anticipated since at the work of Raghavan et al [19], the tuning range (i.e. the maximum and minimum value of G' achieved after tuning) shrinks as the material at rest has its storage modulus increased (either with the increase of weight fraction or with the addition of salt).

The next system of interest was the 7% silica-PEO-LiTFSI blend. Both steady (Figure 3.12b) and oscillatory (Figure 3.12a) preshear experiments were attempted. We can confirm that preshear history can definitely impact the recovered storage modulus increasing it almost by a factor of 3 in the steady preshear case. It is also interesting to point out that all G'/G'_{rejuv} points lie near unity in the oscillatory preshear experiments and take values both below and above one, yet in the steady preshear case, G' always surpasses G'$_{rejuv}$. This could have been anticipated, if we

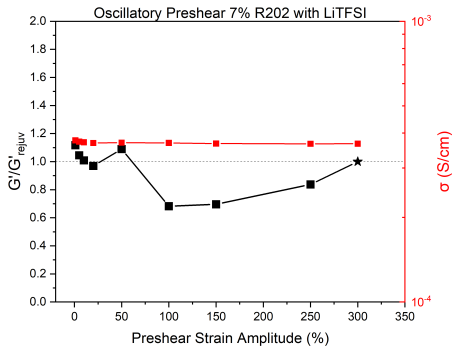

(a) 5min of oscillatory preshear. The rejuvenation was 5 minutes of oscillatory shear at 300%, the DTSs were at 1rad/s and 0.8 strain amplitude, both for 20 minutes and the preshear was applied at a frequency of 1 rad/s

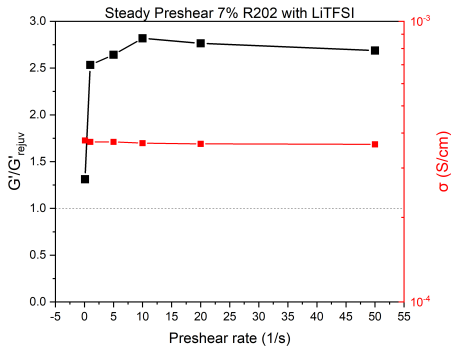

(b) 5 min of steady preshear. The rejuvenation was 5 minutes of oscillatory shear at 300%, and the DTSs were at 1rad/s and 0.8 strain amplitude for 20 minutes

Figure 3.12: Tuning (steady and oscillatory) of 7% R202 in PEO-dme 0.5k with LiTFSI

consider the "rejuvenation" of this sample. Due to shear fracture, an oscillatory shear with strain amplitude of 300% was chosen to initialize the samples. Although this procedure is enough to ensure reproducible results, it is not enough to properly rejuvenate the sample. That means that maximum aggregate breakdown has not been achieved and G'_{rejuv} will definitely be lower than the recovered G' after a steady preshear. In any case, as far as the conductivity is concerned, it remains practically constant, both in the oscillatory and the steady preshear case, corroborating with our previous conclusion, that mechanical and electrochemical properties are decoupled.

Additionally, steady tuning of the 7% PEO-silica-LiTFSI composite was tested, that involves 1h of steady preshear (Figure 3.13), instead of 5 minutes, using the same rejuvenation protocol as before. The x-axis is logarithmic in order to properly visualize all points below 1 s^{-1}. Qualitatively, figures 3.12b and 3.13 are the same, yet in the 1 hour-long preshear case, preshear rates under $1s^{-1}$ have been tested. Here, we observe that for rates lower than $0.1s^{-1}$, the recovered modulus becomes lower than the rejuvenated one. This implies that rates below $0.1s^{-1}$ are not able to break down the aggregates as efficiently as the initial oscillatory shear with strain amplitude of 300% and frequency of 1 rad/s. We could therefore conclude that, in this particular system, a steady shear of approximately $0.12s^{-1}$ (the rate where G' becomes equal to G'_{rejuv}) is equivalent to an oscillatory shear of 300% and frequency

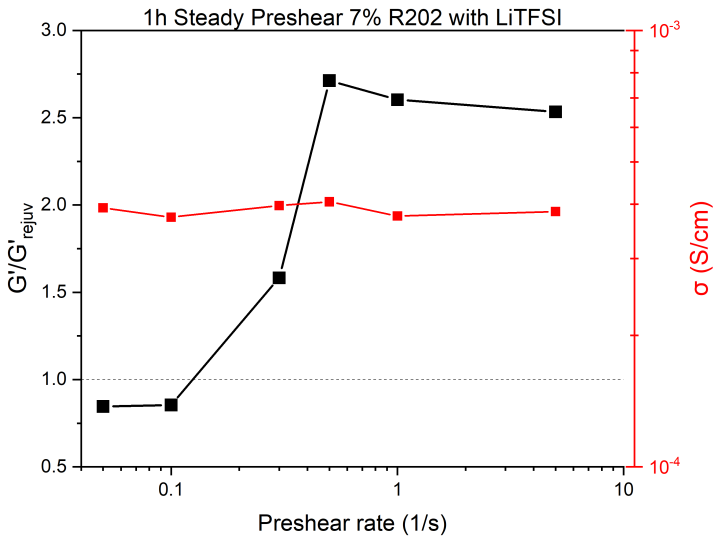

Figure 3.13: 1h steady preshear of 7% R202 in PEO-dme 0.5k with r=0.055 LiTFSI

of 1 rad/s. Once again, conductivity remains constant for the most part and always stays above the desired threshold of $10^{-4} S/cm$(fluctuations are more prominent in this test: this is due to the fact that many gap adjustments had to be made in order to ensure a cylindrical sample between the parallel plates).

Conclusions and Outlook

In this thesis, low molecular weight PEO was added hydrophobic fumed silica nanoparticles, along with LiTFSI in order to prepare battery grade composite polymer electrolytes. Rheology of the composites with and without lithium salt indicates a gel-like behaviour, as indicated by the frequency independent elastic plateau. Increase of the volume fraction of the silica particles yields composites with much higher elastic moduli, while reducing the conductivity by a negligible factor. DSC measurements confirm that both the addition of silica and salt particles inhibit crystallization of the PEO. Additionally, these materials are prone to shear history effects, which was proven by their tunability, both by steady and oscillatory shear. Tuning the microstructure, however showed that electrochemical properties are not compromised by enhanced mechanical properties, thus the decoupling of mechanical and electrochemical properties is confirmed.

Following this work, there are plenty of paths to be explored. The obvious is examining whether further increasing the silica weight fraction still does not compromise conductivity and crystallinity (a non-monotonic behaviour has been observed in higher molecular weight PEO [26]). Also, more rigorous tuning protocols should be devised, including different shear histories, in order to explore if shearing the sample can result in G' higher than the one at rest. Microscopy could be used to visually observe the microstructural changes. Additionally, fumed silica with different surface chemistries should be tested, especially the hydrophilic ones that are reported to form sols in PEO, but stronger gels than the hydrophobic ones in PEO-dme [30].

Bibliography

[1] R. Borah, F.R. Hughson, J. Johnston, and T. Nann. On battery materials and methods. *Materials Today Advances*, 6:100046, June 2020.

[2] Emmanouil Glynos, Christos Pantazidis, and Georgios Sakellariou. Designing All-Polymer Nanostructured Solid Electrolytes: Advances and Prospects. *ACS Omega*, 5(6):2531–2540, February 2020. Publisher: American Chemical Society.

[3] Naoki Nitta, Feixiang Wu, Jung Tae Lee, and Gleb Yushin. Li-ion battery materials: present and future. *Materials Today*, 18(5):252–264, June 2015.

[4] Xiang-Wu Zhang, Yangxing Li, Saad A. Khan, and Peter S. Fedkiw. Inhibition of Lithium Dendrites by Fumed Silica-Based Composite Electrolytes. *Journal of The Electrochemical Society*, 151(8):A1257, July 2004.

[5] Charles Monroe and John Newman. The Impact of Elastic Deformation on Deposition Kinetics at Lithium/Polymer Interfaces. *Journal of The Electrochemical Society*, 152(2):A396, January 2005. Publisher: IOP Publishing.

[6] Wen-Shiue Young, Wei-Fan Kuan, and Thomas H. Epps, III. Block copolymer electrolytes for rechargeable lithium batteries. *Journal of Polymer Science Part B: Polymer Physics*, 52(1):1–16, 2014. _eprint: https://onlinelibrary.wiley.com/doi/pdf/10.1002/polb.23404.

[7] Liping Yue, Jun Ma, Jianjun Zhang, Jingwen Zhao, Shanmu Dong, Zhihong Liu, Guanglei Cui, and Liquan Chen. All solid-state polymer electrolytes for high-performance lithium ion batteries. *Energy Storage Materials*, 5:139–164, October 2016.

[8] H.J Walls, Jian Zhou, Jeffrey A Yerian, Peter S Fedkiw, Saad A Khan, Micah K Stowe, and Gregory L Baker. Fumed silica-based composite polymer electrolytes: synthesis, rheology, and electrochemistry. *Journal of Power Sources*, 89(2):156–162, August 2000.

[9] Saad A. Khan, Gregory L. Baker, and Sandrine Colson. Composite Polymer Electrolytes Using Fumed Silica Fillers: Rheology and Ionic Conductivity. *Chemistry of Materials*, 6(12):2359–2363, December 1994.

[10] Srinivasa R. Raghavan, Jun Hou, Gregory L. Baker, and Saad A. Khan. Colloidal Interactions between Particles with Tethered Nonpolar Chains Dispersed in Polar Media: Direct Correlation between Dynamic Rheology and Interaction Parameters. *Langmuir*, 16(3):1066–1077, February 2000.

[11] George Zardalidis, Dimitrios Chatzogiannakis, Emmanouil Glynos, and Filippos Farmakis. Electrochemical Impedance Spectroscopy Study of Surface Film Formation on Lithium Anodes and the Role of Chain Termination on Poly(Ethylene Oxide) Electrolytes. *ACS Applied Energy Materials*, 4(7):6815–6823, July 2021.

[12] Vanchiappan Aravindan, Joe Gnanaraj, Srinivasan Madhavi, and Hua-Kun Liu. Lithium-Ion Conducting Electrolyte Salts for Lithium Batteries. *Chemistry – A European Journal*, 17(51):14326–14346, 2011. _eprint: https://onlinelibrary.wiley.com/doi/pdf/10.1002/chem.201101486.

[13] Maritza Volel, Michel Armand, and Wladimir Gorecki. Influence of Sample History on the Morphology and Transport Properties of PEO-Lithium Salt Complexes. *Macromolecules*, 37(22):8373–8380, November 2004.

[14] Wenxuan Hu, Yufan Peng, Yimin Wei, and Yong Yang. Application of Electrochemical Impedance Spectroscopy to Degradation and Aging Research of Lithium-Ion Batteries. *The Journal of Physical Chemistry C*, 127(9):4465–4495, March 2023.

[15] Jan Mewis and Norman J. Wagner. *Colloidal Suspension Rheology*. Cambridge University Press, 2012.

[16] Winslow H. Herschel and Ronald Bulkley. Konsistenzmessungen von Gummi-Benzollösungen. *Kolloid-Zeitschrift*, 39(4):291–300, August 1926.

[17] C. Berthier, W. Gorecki, M. Minier, M. B. Armand, J. M. Chabagno, and P. Rigaud. Microscopic investigation of ionic conductivity in alkali metal salts-poly(ethylene oxide) adducts. *Solid State Ionics*, 11(1):91–95, September 1983.

[18] George Zardalidis, Eirini Ioannou, Stergios Pispas, and George Floudas. Relating Structure, Viscoelasticity, and Local Mobility to Conductivity in PEO/LiTf Electrolytes. *Macromolecules*, 46(7):2705–2714, April 2013. Publisher: American Chemical Society.

[19] Srinivasa R. Raghavan and Saad A. Khan. Shear-induced microstructural changes in flocculated suspensions of fumed silica. *Journal of Rheology*, 39(6):1311–1325, November 1995.

[20] Ahmed Helal, Thibaut Divoux, and Gareth H. McKinley. Simultaneous Rheoelectric Measurements of Strongly Conductive Complex Fluids. *Physical Review Applied*, 6(6):064004, December 2016.

[21] Jiang Fan and Peter S. Fedkiw. Composite Electrolytes Prepared from Fumed Silica, Polyethylene Oxide Oligomers, and Lithium Salts. *Journal of The Electrochemical Society*, 144(2):399, February 1997. Publisher: The Electrochemical Society, Inc.

[22] E. van der Aerschot and J. Mewis. Equilibrium properties of reversibly flocculated dispersions. *Colloids and Surfaces*, 69(1):15–22, November 1992.

[23] Changyu Tang, Ken Hackenberg, Qiang Fu, Pulickel M. Ajayan, and Haleh Ardebili. High Ion Conducting Polymer Nanocomposite Electrolytes Using Hybrid Nanofillers. *Nano Letters*, 12(3):1152–1156, March 2012.

[24] Richard Buscall, Paul D. A. Mills, James W. Goodwin, and D. W. Lawson. Scaling behaviour of the rheology of aggregate networks formed from colloidal particles. *Journal of the Chemical Society, Faraday Transactions 1: Physical Chemistry in Condensed Phases*, 84(12):4249, 1988.

[25] Srinivasa R. Raghavan, Michael W. Riley, Peter S. Fedkiw, and Saad A. Khan. Composite Polymer Electrolytes Based on Poly(ethylene glycol) and Hydrophobic Fumed Silica: Dynamic Rheology and Microstructure. *Chemistry of Materials*, 10(1):244–251, January 1998.

[26] Kwang-Sun Ji, Hee-Soo Moon, Jong-Wook Kim, and Jong-Wan Park. Role of functional nano-sized inorganic fillers in poly(ethylene) oxide-based polymer electrolytes. *Journal of Power Sources*, 117(1-2):124–130, May 2003.

[27] W. Wieczorek, Z. Florjanczyk, and J. R. Stevens. Composite polyether based solid electrolytes. *Electrochimica Acta*, 40(13):2251–2258, October 1995.

[28] E. Drabarek, J.R. Bartlett, H.J.M. Hanley, J.L. Woolfrey, C.D. Muzny, and B.D. Butler. Shear-Induced Restructuring of Colloidal Silica Gels. *Journal of Sol-Gel Science and Technology*, 19(1):279–283, December 2000.

[29] Esmaeel Moghimi, Alan R. Jacob, Nick Koumakis, and George Petekidis. Colloidal gels tuned by oscillatory shear. *Soft Matter*, 13(12):2371–2383, 2017.

[30] Srinivasa R. Raghavan, H. J. Walls, and Saad A. Khan. Rheology of Silica Dispersions in Organic Liquids: New Evidence for Solvation Forces Dictated by Hydrogen Bonding. *Langmuir*, 16(21):7920–7930, October 2000.